THE JOURNAL OF PHYSICAL CHEMISTRY C
A JOURNAL OF THE AMERICAN CHEMICAL SOCIETY

pubs.acs.org/JPCC

Article

Plasmonic Enhancement of Local Fields in Ultrafine Metal Nanoparticles

Lasse K. Sørensen, Anton D. Utyushev, Vadim I. Zakomirnyi, Valeriy S. Gerasimov,* Alexander E. Ershov, Sergey P. Polyutov, Sergey V. Karpov, and Hans Ågren*

Cite This: *J. Phys. Chem. C* 2021, 125, 13900−13908

Read Online

ACCESS | Metrics & More | Article Recommendations

ABSTRACT: We present an analysis of ultrafine metallic nanoparticles (1−15 nm) with respect to electromagnetic field generation by plasmonic excitations. A number of structures with different symmetries and geometries are studied in order to analyze the distributions of plasmonically generated near-electric fields and the concentration of hot and cold spots around the particles. The study is made possible by the recent development of an extended discrete interaction model (Ex-DIM) where the explicit dependency of the plasmonic spectra on the structure and composition of particles in the range of 1−15 nm is accounted for. With the Ex-DIM, the optical response of the internal crystal structure of the nanoscale particles can be visualized, thereby making it possible to predict the dependence of the generated local fields with respect to the position of the particles relative to the external field polarization. The results indicate rather surprising concentrations of the plasmon fields in very confined hot spots also in cases when the particles retain a high symmetry. The consequence of the findings of this study when using small symmetric nanoparticles for near-field imaging is briefly discussed.

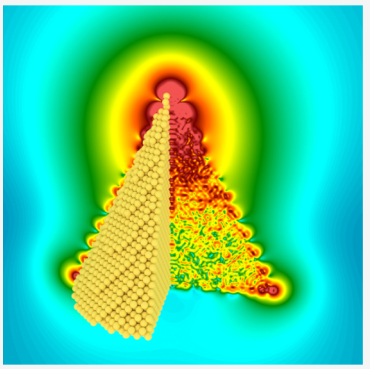

INTRODUCTION

The important features of nanoplasmonics are the combination of a giant enhancement of electromagnetic fields in a wide spectral range and their strong localization around nanoparticles. Plasmonic nanoparticles are frequently employed as modifiers of the optical properties of various optically sensitive objects and materials, such as molecules, their aggregates, and quantum dots.[1] At the same time, the properties of localized plasmons critically depend on the shape of the nanoparticles, which makes it possible to tune their resonance system to effectively interact with light or with other quantum objects. Such properties of plasmonic nanoparticles have enabled the discovery of a number of new effects. First of all, giant local fields near nanoparticles result in an increase in the Raman cross section by 10−14 orders of magnitude, which makes it possible to observe individual molecules and to develop methods for determining their structure.[2] Plasmonic nanoparticles provide simultaneous enhancement of extinction and emission of light and, thus, effectively replace fluorophores and nanoscale light sources, including nanolasers.[3−6]

The localization of the strong local fields is known to be associated with collective electron excitations generating surface plasmon resonances (SPRs) that depend on the geometric properties of the particles.[7,8] The plasmonic optical response thus depends on the material, the shape, and the size of the nanoparticles which, in their presence, can be used to tune the optical properties of a molecular dye located in the vicinity of the surface of the metallic particle. The locally enhanced fields are the basis for increasing the sensitivity of spectral methods for determining the chemical composition of impurity materials up to the level of single molecules.[1,9] This fact also lays the basis for a number of applications in bioimaging,[10−12] nanosensing,[9,13,14] nanophotonics,[15−17] and medicine;[18] see also works by Halas[19] and Linic[20] for further details.

The applications alluded to the above have been greatly boosted by the advances in nanofabrication techniques, which have made it possible to control the variation in the shape and size of the particles and their material content.[21] Traditional technologies for the chemical synthesis of nanoparticles based on colloidal systems have been complemented by fabrication based on pulsed laser ablation of bulk materials in liquid media and by the synthesis of self-organizing nanoparticles in gaseous media, which have made it possible to fabricate nanoparticles upon their deposition on a substrate.[22−25] Furthermore, technologies have been developed for fabricating nanoparticles and synthesis of periodic arrays by both sputtering onto a substrate from the gas phase through nanomasks and by

Received: February 16, 2021
Revised: June 2, 2021
Published: June 16, 2021

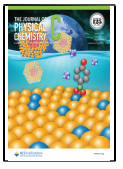

https://doi.org/10.1021/acs.jpcc.1c01424
J. Phys. Chem. C 2021, 125, 13900−13908

directional etching of various shapes on the faces of single-crystal samples.[26−29]

The tuning of plasmonic properties are well known for somewhat larger particles (>20 nm); red-shifting, deep into the infrared region, follows with size; blue shifting can be introduced by alloying;[30,31] multiple resonances can be introduced by non-spherical particles with different aspect ratios;[32] hot spots can be triggered by field concentrations at sharp edges.[7] For example, in scanning tunneling microscopy applications, the plasmon fields are mostly located at the very top of the tips, making an ultrastrong field enhancement possible there.[33] The plasmon generation and the field anisotropy can be controlled by tuning the structure of the nanoparticle—the simplest case here is nanorods.[32] All these aspects, which thus are supported by modern controlled synthesis, have opened important perspectives in terms of optical applications in a wide wavelength range.

The development of nanoparticle technology has, however, been slowed by a concomitant development of theoretical tools for the nanoparticle design with respect to plasmonic excitations, which so far has been quite limited in the small size region. Although there are developments "from above" by so-called non-local finite-difference time-domain (FDTD) theories[34,35] and "from below" by quantum time-dependent DFT models,[36] there is still a size gap to fill. The large surface to volume ratio and confinement of the mean free path of the conduction electrons impose limitations to classical models based on the bulk dielectric constant for their use toward nanoparticles in the small size region, while quantum methods effectively cannot reach beyond 1 nm with accurate functionals. Here, in the gap region, discretization of the interactions is called for down to the atomic level in ways that can describe the dependence of the polarizability of the surface topology or structure of the metallic nanoparticles. However, the original discrete interaction models, assuming that the atom polarizabilities themselves are constant throughout the particle, are also limited in application, especially concerning the dependence of the polarizability of the surface topology of the metallic nanoparticles and in studies of the polarizability of composite nanoparticles.

An important contribution to discrete interaction models going beyond fixed atom polarizabilities was given by Chen et al.[37] who presented a discrete interaction model where the polarizabilities were made coordination-dependent. Recently, we presented the "extended discrete interaction model" (Ex-DIM),[38] giving the possibility to simulate the geometric dependence of plasmons of small nanoparticles. This is carried out by replacing the frequency-dependent dielectric function from the Clausius−Mossotti relation by a static atomic polarizability times the sum of three size-dependent Lorentzian oscillators with Gaussian charge distributions and atomic radii that vary with the coordination number. The frequency-dependent Lorentzian oscillators depend here on the plasmon length along the three Cartesian directions using the concept of the plasmon length as defined in the work of Ringe et al.[39] As shown in our work, the Ex-DIM, parameterized versus experimental data, enables a good description of the polarizability of small nanoparticles with different geometries, thereby allowing the dependency of the generated plasmon to a specific structure of the nanoparticles to become unraveled.[31,38,40]

Employing the new possibilities that the extended discrete interactions model offers, we intend with the present paper to explore how plasmon-induced electromagnetic fields distribute and concentrate for different kinds of geometric shapes and symmetries of smaller (1−15 nm) nanoparticles. We are in particular interested in how hot spot generation can be induced by anisotropy effects, and the dependence of their strength and size with respect to the symmetry of the particles and with respect to the direction of the applied field.

New nanotechnologies have awakened interest in the study of the properties of nanoparticles of various types, differing in size, shape, and material.[41−43] Furthermore, the conventional discrete dipole interaction models, despite the atomistic nature, have limited capabilities to describe the dependence of the plasmon polarizability on the surface topology of the metallic nanoparticles and to study the polarizability of composite nanoparticles. Thus, the detailed field generation of smaller nanoparticles has still remained an open issue.

MODEL

The Ex-DIM[38,40] is a discrete structure model where each atom is represented by a Gaussian charge distribution and endowed with a polarizability, which govern the inter-atomic interaction.[44−47] The Ex-DIM here improves the description of the surface topology geometric dependence in comparison to older discrete interaction models. The parameterization also differs since the Ex-DIM is parameterized directly from experimental data, noting that extrapolation of data from quantum mechanical methods and classical methods into the 1−15 nm size range, where the Ex-DIM applies, does not appear to be feasible currently.[38]

The Lagrangian is written in the usual form as the interaction energy E minus the charge equilibration constraint expressed via the Lagrangian multiplier λ

$$L_0[\{\boldsymbol{\mu}, q\}, \lambda] = E[\{\boldsymbol{\mu}, q\}] - \lambda\left(q^{\mathrm{tot}} - \sum_i^N q_i\right) \tag{1}$$

where N is the number of atoms, q_i is the fluctuating charge assigned to the i-th atom, and q^{tot} is the total charge of the nanoparticle. The interaction energy $\mathrm{E}[\{\boldsymbol{\mu}, \mathrm{q}\}]$ in this way captures all different types of interactions involving fluctuating dipoles $\boldsymbol{\mu}$, charges q, and an external field.[38] A coordination number, as defined by Grimme,[48] is assigned to each atom and aids the description of the surface topology, which becomes important when the surface to bulk ratio changes. The coordination number f_{cn} modifies the atomic polarizability through the scaling of the radius

$$\boldsymbol{\alpha}_{ii,kl}(\omega) = \left(\frac{R_i(f_{\mathrm{cn}})}{R_{i,\mathrm{bulk}}}\right)^3 \alpha_{i,s,kl} L(\omega, \mathbf{P}) \tag{2}$$

In eq 2, $R_{i,\mathrm{bulk}}$ is the bulk radius of the atom, $R_i(f_{\mathrm{cn}})$ is the coordination number scaled radius,[38] $\boldsymbol{\alpha}_{i,s,kl}$ is the static atomic polarizability,[49] and $L(\omega, \mathbf{P})$ is a size-dependent Lorentzian. In order to take into account the contribution of interband transitions, we added a combination of two additional Lorentzian terms in eq 2 with parameters taken from ref 50. The size-dependent interband transitions are extrapolated from the fit to the experimentally measured interband transitions.[50] Since the experimental data for the larger particles (>10 nm) was limited at 300 nm, the validity of the fit of the interband transitions for particles for larger particles is also limited at 300 nm. Having two Lorentzians to describe the interband transition can occasionally result in minor peaks in the interband as seen in Figure 1.

https://doi.org/10.1021/acs.jpcc.1c01424
J. Phys. Chem. C 2021, 125, 13900−13908

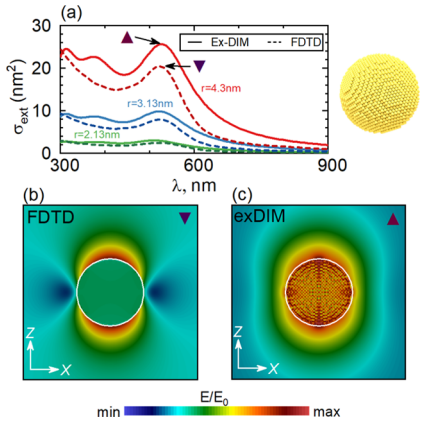

Figure 1. Extinction cross-section spectra for spherical Au nanoparticles of different sizes in an aqueous medium calculated by the Ex-DIM (solid lines) and by the FDTD methods (dashed lines). Configuration of the local electric field calculated for spherical particles with r = 4.3 nm using the FDTD method (b) and Ex-DIM (c) for Au spherical particles at the wavelength λ = 525 nm.

The geometric dependence of the SPR is determined by the size-dependent Lorentzian $L(\omega, \mathbf{P})$

$$L(\omega, \mathbf{P}) = N(L_x(\omega, P_x) + L_y(\omega, P_y) + L_z(\omega, P_z)) \tag{3}$$

where each Lorentzian depends on the plasmon length P_i[39] in the given direction

$$\omega_i(P_i) = \omega_a(1 + A/P_i) \tag{4}$$

and in this way, cluster size dependence and complicated geometrical shapes, with up to three SPRs, can be simulated for solid particles. Here, ω_a and A are the atomic-specific resonance frequency and size dependence, respectively, which are fitted from the experiment.[38]

The frequency-dependent polarizabilities from the fluctuating dipoles $\boldsymbol{\mu}$ are determined by applying a weak uniform electric field $\mathbf{E}$

$$\mathbf{A}\boldsymbol{\mu} = \mathbf{E} \tag{5}$$

Here, $\mathbf{A}$ is defined as

$$\mathbf{A}_{ij} = \delta_{ij}\boldsymbol{\alpha}_{ij}^{-1} - (1 - \delta_{ij})\mathbf{T}_{ij}^{(2)} \tag{6}$$

where $\boldsymbol{\alpha}_{ij}$ is defined in eq 2 and $\mathbf{T}_{ij}^{(2)}$ is the electrostatic interaction tensor between dipoles.[51] Eq 5 is solved using the generalized minimal residual iteration method with accelerated convergence (LGMRES) since we were unable to converge the conjugate gradient methods with sufficient accuracy.[52] Using the LGMRES algorithm instead of inverting the relay matrix in eq 5 has resulted in a more than a factor 100 speed-up of the calculation of the frequency-dependent polarizability. The time per frequency for a 17,549 atom nanoparticle can in this way be reduced to 44 s on a single 32 core compute node. The extinction cross section was calculated using the following equation

$$\sigma_{ext} = 4\pi k\frac{\mathrm{I}(\mu\cdot\mathbf{E}_0^*)}{|\mathbf{E}_0|^2} \tag{7}$$

From the atomic dipole moments, obtained by the Ex-DIM, the configuration of the electromagnetic field inside and outside the nanoparticle can be calculated. According to the Lorentz approach,[53] the atoms immersed in a vacuum create an electric field, called the microscopic field, which is the total field created by the dipole moments of each atom taking into account the Gaussian charge distribution

$$\mathbf{E}(\mathbf{r}) = \mathbf{E}_0 + \sum_i \int\int\int_V \mathbf{T}(\mathbf{r} - \mathbf{r}')\mathbf{d}_i(\mathbf{r}')d^3\mathbf{r}' \tag{8}$$

Here, $\mathbf{E}_0$ is the external field, $\mathbf{d}_i(\mathbf{r})$ is the distribution of the i-th particle's dipole moment, $\mathbf{r}$ is the radius vector, and second-order tensor $\mathbf{T}$ reads as follows

$$\mathbf{T}(\mathbf{r}) = \frac{3\mathbf{r}\otimes\mathbf{r} - r^2\mathbf{I}}{r^5} \tag{9}$$

where $\mathbf{I}$ is the unit tensor.

Using eq 13 in ref 54, where $R_\mu^j \to 0$, an explicit expression for the field is given as

$$\mathbf{E}(\mathbf{r}) = \mathbf{E}_0 + \sum_i \left(A\frac{I}{{R_i}^2} + B\frac{\mathbf{R}_i\otimes\mathbf{R}_i}{{R_i}^5}\right)\boldsymbol{\mu}_i$$

$$A = \frac{2\sqrt{a}R_i}{\sqrt{\pi}e^{a{R_i}^2}} - \mathrm{erf}(\sqrt{a}R_i)$$

$$B = 3\mathrm{erf}(\sqrt{a}R_i) - \frac{4a^{3/2}{R_i}^3 + 6\sqrt{a}R_i}{\sqrt{\pi}e^{a{R_i}^2}}$$

$$\mathbf{R}_i = \mathbf{r} - \mathbf{r}_i \tag{10}$$

The core module of the field calculation program is designed in pure C programming language as the dynamic library for the highest multi-thread efficiency and frontend module in Python. The program is capable of calculating high-resolution 3D complex field maps and storing them in open-source spatial data format VTK (Visualization Toolkit) as a structured grid.[55] The atomic structure of the nanoparticles was obtained from an ideal face-centered lattice by cutting out a stereolithography file that defines the shape of the particle using the open-source Paraview software.[56]

To verify the optical properties of the nanoparticles obtained with the Ex-DIM, we employed a commercial FDTD package,[57] where the FDTD simulation utilized a plane wave illumination. Perfectly matched layer boundary conditions were used on all sides of the simulation cell and the total field scattered field (TFSF) technique was utilized to reproduce infinite space. The absorption cross section has been calculated with the set of discrete Fourier transform (DFT) monitors surrounding the particle inside the TFSF region while the scattering cross section is obtained with the monitors surrounding the entire TFSF region so that they read only the scattered field. An adaptive mesh has been used to accurately reproduce the particles' shape.

RESULTS

As a start, we will examine spherical Au plasmonic particles since these are well known and can be used as objects for verification and correlation with calculations by FDTD and experimental data for moderate-sized particles along with the parameterization approach of the Ex-DIM. This is followed by a characterization of plasmonic nanoparticles of arbitrary shapes and analysis of plasmon extinction spectra and distribution patterns of the local electromagnetic field in the vicinity of the particles.

The comparisons with experiments often show that classical electromagnetic theory works well provided that there is a good

https://doi.org/10.1021/acs.jpcc.1c01424
J. Phys. Chem. C 2021, 125, 13900−13908

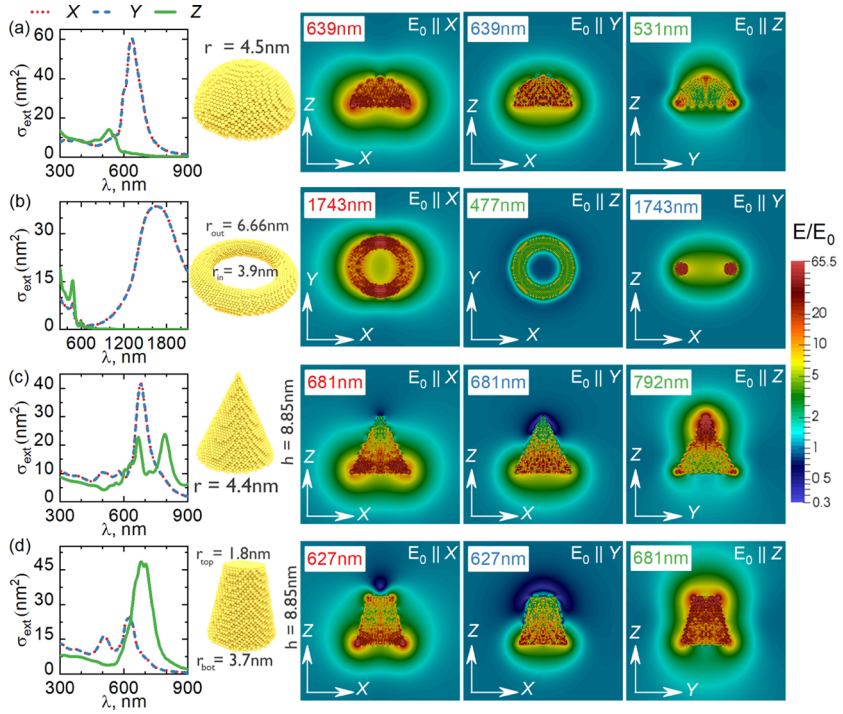

Figure 2. Extinction cross-section spectra of Au nanoparticles and electric-field distributions at the resonant maximum for different shapes: (a) hemisphere, (b) torus, (c) cone, and (d) truncated cone. The color designation of the wavelength in each frame corresponds to the color of the spectral curves obtained for different polarizations. All nanoparticles contain approximately the same number of atoms ~10^4. Geometrical parameters of the particles are specified in the text.

measurement of the particle structure and provided that the complex dielectric environment is properly characterized and modeled (see Figures 1−3). However, this contention applies only when the considered particles are large enough that the size dependence of the dielectric constant is not an issue, and for smaller particles this will indeed be an important factor. Furthermore, the conventional discrete dipole interaction models, despite the atomistic nature, have limited capabilities to describe the dependence of the plasmon polarizability of the surface topology of the metallic nanoparticles and to study the polarizability of composite nanoparticles. Thus, the detailed field generation of smaller nanoparticles has still remained an open issue.

Figures 2 and 3 demonstrate the features of the plasmonic extinction spectra of Au particles with complex shapes modeled with the Ex-DIM. The figures show strong deviation from Lorentzian surface plasmon extinction spectra typical for ideal spherical particles. The deviation from the Lorentzian surface plasmon extinction spectra is especially seen in particles with complex shapes and sharp edges. These shape features can significantly change spectra which acquire a multimodal composition.

Spherical Particles. The extinction cross sections of spherical nanoparticles shown in Figure 1a and the field distribution in their vicinity in Figure 1b,c are largely interrelated. The absence of sharp edges manifests itself in smooth gradients of the local field strength. Figure 1c shows the fine atomistic structure of the local field distribution. Hot spots arise only at poles in the direction of polarization of the incident radiation.[58] A cold area emerges around the equatorial part of a sphere, the origin of which, apparently, has an interference nature under conditions which can be destructive between the external and the plasmonic fields. Spherical particles are characterized by a smooth Lorentzian form-factor of the surface plasmon extinction band due to the symmetry of the particle. In cases of symmetry breaking, as for nanorods or prolate spheroids, the spectra are characterized by two maxima—a weaker transverse and an intense longitudinal polarization (in the case of a transverse size less than 2 nm, the resonance of this configuration is not observed).[38]

Non-Spherical Particles with a Complex Shape: Plasmonic Extinction Spectra and Local-Field Distributions. Besides the most widespread studied spheres and nanorods, non-spherical particles arise during experimental synthesis and can be used in various applied problems. The sources of the distinctive features of extinction spectra of the nanoparticles of a complex shape are the sharp edges with a minimum radius of curvature, in which the electron density considerably increases in the field of an electromagnetic wave that causes significant enhancement of the local field (Figures 2 and 3).

Hemispherical Particles. The extinction spectra of Au hemispheres in transverse (X, Y) polarization in Figure 2a noticeably differ from spherical particles (Figure 1a) in the position of the plasmon resonance, which is shifted to longer wavelengths by about 100 nm. For longitudinal (Z) polarization, extinction decreases and is accompanied by a blue shift of the extinction, which coincides with that for the sphere. In addition, the structure of the local field differs from the classical picture of the dipole field of a sphere (Figure 1) due to the presence of a sharp edge around the bottom of the hemisphere. The available experimental data for the plasmonic Ag hemispheres[59] demonstrate the same tendencies and general similarity.

Toroidal Particles. Toroidal nanoparticles are well described in the literature[60] and are characterized by a smooth and wide extinction curve, shifted to longer wavelengths

https://doi.org/10.1021/acs.jpcc.1c01424
J. Phys. Chem. C 2021, 125, 13900−13908

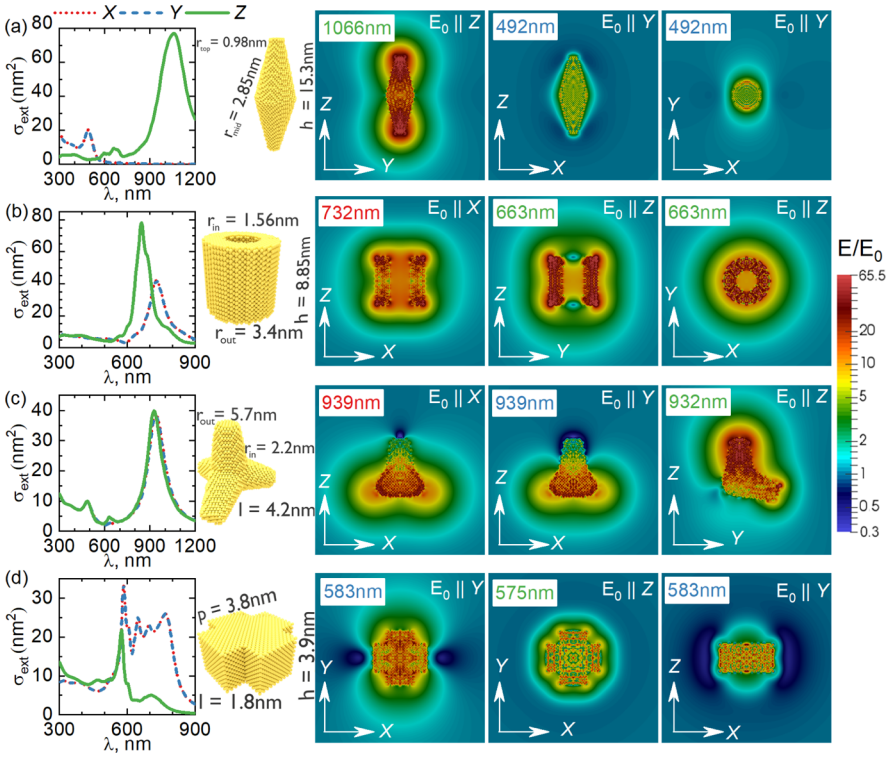

Figure 3. Extinction cross-section spectra of Au nanoparticles and electric-field distributions at the resonant maximum for different geometries: (a) truncated double cone, (b) nanotube, (c) tetrapod, and (d) cross-shaped particle.

compared to spheres with similar widths. The spectral features are also similar to the spectra of nanorods in the case of longitudinal polarization. In experiments, nanotori[60] demonstrate one broad resonance in the visible range. In the Ex-DIM, we, however, clearly notice two resonances as shown in Figure 2b where one resonance is in the near-IR range and the second one is in the short-wavelength range of the visible range. Rings (or tori) of the size given in Figure 2b with R_{out} = 6.66 nm and r_{in} = 3.9 nm have not yet been explored experimentally to the best of our knowledge. However, a seminal paper on rings of the size of ca. 60 nm with varying thicknesses of the ring walls was presented in ref 61, including experimental plasmonic spectra as well as classical calculations of spectra and fields. A substantial red shift of the extinction maximum could be recorded from ca. 1000 to 1400 nm as the ring thickness was lowered from 14 to 9 nm. The same tendency was observed in the work by Mary et al.[60] The spectra for the rings can be analyzed in terms of strong electromagnetic coupling between the inner and outer ring walls when the thickness is small compared to the ring radius. This leads to a scheme of mode splitting, characterized by symmetric and antisymmetric mode branches, similar to the case of hollow metal particles that we studied by the Ex-DIM in ref 61. We note that for the torus shape, the shielding effect of the depolarizing field inside the torus is not observed, which would occur in the case of an enclosed nanobubble.[40] This is especially pronounced in the calculation results obtained by the FDTD method.[40]

The distribution of the fields inside the nanoparticle features cold spots at the poles along the polarization of the external field and hot spots in the orthogonal direction (see, e.g., ref 62). At the same time, the inner cavity is characterized by a constant depolarization field amplitude. This pattern coincides in general with the larger ring particles studied in ref 61. We note that the physics behind the appearance of cold spots refers to the interference between the applied field and the plasmonic field and that the symmetry of the field and particle system can be lower than the symmetry of the particle itself.

Conical and Truncated Conical Particles. A characteristic feature of the extinction spectra of conic particles in longitudinal polarization (Z) is a splitting of the extinction band in the wavelength range, covering the long-wavelength part of the visible and near-infrared range (Figure 2c). In the transverse polarization (X, Y), there is a single maximum with a large amplitude, which is close in position to that for a hemisphere.

The local field distribution is very inhomogeneous and, as expected, is concentrated for different polarizations around sharp edges—around the bottom edge for X, Y-polarizations—and is especially pronounced for Z-polarization in the vicinity of the tip of the cone, Figure 2c. These strong fields appear to be spatially limited and outside these hotspots, the field amplitudes decrease rapidly and even create cold spots due to destructive interference between the generated and the external fields. The distance between hot and cold spots is only of the order of 1 nm, which poses extreme geometric requirements when conical and triangular particles of this size are used as high-field concentrators for detecting impurities in surrounding media. It is noteworthy that a more preferable shape of the field concentrations can be obtained using two cones directed toward each other, connected by bottom parts with a ring or torus as a large reservoir of conduction electrons. In this case, we predict a maximum enhancement of the field between the tips of the cones due to the redistribution of conduction electrons in the real particles at the tips with the maximum achievable concentration.

As for the truncated cone in Figure 2d, its extinction spectrum for longitudinal polarization (Z), in contrast to the spectrum of the original cone, is transformed into a mono-resonant peak with a large amplitude. The presence of two peaks for transverse polarization (X, Y) is due to two characteristic dimensions,

https://doi.org/10.1021/acs.jpcc.1c01424
J. Phys. Chem. C 2021, 125, 13900−13908

namely, the radii of the upper cut and the base of the cone. Attention can be drawn to the high localization of the field near the sharp edges around the base and the top.

Truncated Double-Conical Particles. The truncated double cone in Figure 3a has a general resemblance to the truncated cone shape particle discussed above. However, despite this fact, their optical properties differ significantly. The truncated version of a double cone was chosen due to available experimental data on bipyramidal nanoparticles and biconical nanoparticles with blunt tips.[7,42] However, there are no experimental data for this shape with sharp tips. In longitudinal polarization (Z), we find in the extinction spectrum a mono-resonant long-wavelength extinction band with a large amplitude and a maximum at a wavelength of about 1000 nm. In transverse polarization (X, Y) for large values of the aspect ratio, the maximum lies near 450 nm and its amplitude is much smaller than that of the longitudinal polarization. In the case of small values of the aspect ratio, the amplitude of the extinction band grows in the transverse polarization direction; simultaneously, it decreases for the longitudinal polarization.

Importantly, the position of the maximum in the extinction spectrum of the double cone strongly depends on both the radius of curvature of the tips and the aspect ratio of a particle. The larger the aspect ratio, the larger the red shift of the extinction maximum. The more the tip of a cone is cut off, the more the extinction spectrum maximum shifts to the short wavelength range. A less pronounced effect of the size of the double cone particle on the position of the maximum is also observed.[42] As the particle size is reduced, the maximum shifts to the short-wavelength range, and its amplitude decreases. Both FDTD theory and experiment presented in ref 42 applied to large bipyramids (or double-cones) suggest that a larger radius of curvature, where "radius" is the radius of a cut rounded tip, results in a blue-shifted longitudinal LSPR peak, in fact in a linear relationship if the length of the bipyramid is constant. Conversely, particles of constant radius of tip curvature will see red-shifted longitudinal resonance peaks for a longer particle length. Although here we deal with a much smaller size, these results confirm the great sensitivity to how the tip of the cone is cut.

Figure 3a shows the spatial distribution of the electric field in a truncated double-cone Au structure. As expected, the field is strongly enhanced in the vicinity of the sharp tips, while it is low near the central part of the structure. Nanoparticles represented here are examples of structures in which most favorable conditions arise for strengthening the local field near the tips. In the classical interpretation, the maximum concentration of conduction electrons is reached in the tips, which creates a maximum field strength. The smaller the volume of the tip and the smaller its curvature radius, the higher the field strength for a longitudinal polarization of the field.

Tubular Particles. Au nanotubes offer new potential advantages that can be exploited in theranostic applications that integrate targeting, imaging, and therapy into one platform.[63] Thus many applications of Au nanotubes have been used in biosensing, protein transportation, photothermal therapy, and imaging.[64] First, open-ended nanotubes have large inner voids considered as containers that can be filled with suitable drugs for targeted delivery in methods of chemotherapy. Second, compared to their spherical counterparts, the elongated nanotubes have extinction bands in the spectral range of transparency of hemoglobin that makes it possible to use them for laser photothermal therapy and hyperthermia of malignant cells. Besides that, nanotubes[65] have been shown to have great potential for SERS probing and they may be used as nanofluidic devices to transport solutions to or from cells.

These advantageous features of nanotubes warrant a thorough study using Ex-DIM techniques to optimize their sensing capabilities; however, as we consider many geometric shapes in this paper, we study here only one particular Au nanotube with an outer radius of 3.4 nm, an inner radius of 1.56 nm, and a height of 6.8 nm. Figure 3b shows that the extinction band maxima in the spectra of this nanotube for longitude (Z) and transfer (X, Y) polarization lie in the wavelength range larger than 660 nm, which corresponds to the short wavelength border of the hemoglobin transparency range.[18] As in truncated cones, the local field in nanotubes is concentrated around the outer and inner sharp edges.

Tetrapodic Particles. Nanoparticles in the shape of tetrapods are of particular interest due to the possibility of generating a multimode response because of the presence of several resonator configurations. A tetrapodic nanoparticle is similar to a combination of four rods connected together at one end and oriented at 120° to each other. If classical electromagnetic models were applied to such a figure, one would expect the mutual influence of these limbs on each other, which would inevitably be reflected in the extinction spectrum. This mutual influence will be similar to the interaction of closely spaced plasmonic nanorods in external fields. However, the calculation shows that all three orthogonal orientations have approximately the same response in Au structures, which is clearly seen in Figure 3c. The field configuration for the resonance wavelength λ = 939 nm is shown in Figure 3c. The main features of the field enhancement pattern in tetrapodic nanoparticles refer to the strong field localization near the limbs oriented along the polarization of the external field, while in the orthogonal direction a cold spot can be observed.

Cross-Shaped Particles. Figure 3d shows extinction cross-sectional spectra for small cross-shaped Au nanoparticles. In general, cross-shaped nanoparticles demonstrate a broadened resonant band in the visible red or near-IR part with transverse (X, Y) polarization. With longitudinal polarization, we find a much narrower maximum located at λ = 583 nm with comparable amplitude.

The configuration of a local field in a cross-shaped Au nanoparticle at a maximum extinction wavelength of λ = 575 nm (Z) is shown in Figure 3d. The field shows pronounced cold spots at a distance of several nanometers observed in the Y-polarization.

DISCUSSION

In the present work, we capitalize on the recent development of a discrete interaction model (Ex-DIM) where the explicit dependency of the electromagnetic field-generated plasmonic excitations versus structure and composition of particles in the range 1−15 nm is accounted for. Earlier predictions of spheres, rods, and hollow particles using this model are complemented here by a number of other structures with different symmetries and geometries and, in particular, by predictions of the local distributions of the plasmonically generated electric near-fields for all these particles. Comparison with the FDTD solutions of the Maxwell equations was made for spherical particles. In general, we confirm that also for very small nanoparticles, one observes field localizations and charge concentrations at surfaces and close to sharp edges. However, the Ex-DIM predicts that such localization is spatially very confined, even for high

https://doi.org/10.1021/acs.jpcc.1c01424
J. Phys. Chem. C 2021, 125, 13900−13908

symmetry particles, and that outside such fine hot spots, the field amplitudes rapidly decrease and even generate cold spots as an effect of interfering external and generated fields. The distances between hot and cold spots are only of the order of 1 nm or even less, thus putting extraordinary geometric requirements when particles of this size are employed as strong field concentrators. Local fields near one tip can be additionally enhanced by the tip of the neighboring particle. Such a situation can also be realized within a separate particle of complex shape having two tips pointing toward each other and attached to a common base. This will be the subject of a specialized future study.

A strong point of the Ex-DIM is the possibility it gives to further study the optical response of nanoscale particles and taking into account their internal crystal structure. This makes it possible to predict the dependence of the generated local fields with respect to the external field polarization, something that is not possible with the commonly applied classical models. Similarly to the ultrasmall local hot and cold spot generation, this aspect has an important bearing on the use of small nanoparticles for monitoring defects and molecules. We can here refer the current possibilities for local plasmonic-enhanced Raman images of a single molecule with subnanometer resolution obtained by the tip-enhanced Raman scattering technique.[9] When the spatial distribution of the plasmonic field is comparable to the size of the molecule, the optical transition matrix of the molecule becomes dependent on the position and distribution of the plasmonic field, resulting in spatially resolved high-resolution Raman images which reflect the electronic transition density of the molecule. The physical origin of these images would be understood from the coupled Ex-DIM−quantum mechanics description of the interaction between the molecule and the highly confined plasmonic field, accommodating Raman theory modified for position-dependent electric fields.[14] The plasmonic particles and their confined super-enhanced fields and hot spots could so be designed in the subnanometer scale for obtaining optimal Raman signals and spectra.

It is clear that a limitation of the FDTD method is the use of bulk epsilon constants even for these smaller nanoparticles. Although some corrections for this has commonly been introduced as "quantum corrected" dielectric constants, still the fact that the "true" dielectric constant varies over the particle, for example between the interior and the surface, is ignored. This has motivated us to develop an effective method, which merges the Ex-DIM and FDTD where local, atomic, dielectric constants generated by the Ex-DIM are introduced into the FDTD code—a demonstration of that will be presented in a forthcoming work.

The Ex-DIM method thus allows considerable flexibility toward structural dependence, as we also have proved in two earlier papers for rods and hollow particles.[31,40] This goes for several other structures now including the generated fields also, as presented here. An interesting extension of the present work including also the explore how to explicitly relate plasmon appearance to the internal particle structure, in addition to size, shape, and material content. The Ex-DIM has the inherent capability to explore that aspect as well as the role of temperature chaotization of the crystal parameters and the role of line shape broadening. It is thus clear that the area of plasmonic generation in small nanoparticles still remains wide open, concerning both further method development and applications, two aspects that we intend to work on in the future.

AUTHOR INFORMATION

Corresponding Authors

Valeriy S. Gerasimov − *International Research Center of Spectroscopy and Quantum Chemistry, Siberian Federal University, Krasnoyarsk 660041, Russia; Institute of Computational Modelling, Federal Research Center KSC SB RAS, Krasnoyarsk 660036, Russia;* orcid.org/0000-0002-4540-7408; Email: valkrsk@gmail.com

Hans Ågren − *Department of Physics and Astronomy, Uppsala University, SE-751 20 Uppsala, Sweden; International Research Center of Spectroscopy and Quantum Chemistry, Siberian Federal University, Krasnoyarsk 660041, Russia; Federal Siberian Research Clinical Centre under FMBA of Russia, Krasnoyarsk 660037, Russia;* orcid.org/0000-0002-1763-9383; Email: hagre@kth.se

Authors

Lasse K. Sørensen − *Department of Physics and Astronomy, Uppsala University, SE-751 20 Uppsala, Sweden; Department of Theoretical Chemistry and Biology, School of Engineering Sciences in Chemistry, Biotechnology and Health, Royal Institute of Technology, Stockholm SE-10691, Sweden*

Anton D. Utyushev − *International Research Center of Spectroscopy and Quantum Chemistry, Siberian Federal University, Krasnoyarsk 660041, Russia;* orcid.org/0000-0002-9642-2050

Vadim I. Zakomirnyi − *International Research Center of Spectroscopy and Quantum Chemistry, Siberian Federal University, Krasnoyarsk 660041, Russia; Institute of Computational Modelling, Federal Research Center KSC SB RAS, Krasnoyarsk 660036, Russia;* orcid.org/0000-0002-2049-7259

Alexander E. Ershov − *International Research Center of Spectroscopy and Quantum Chemistry, Siberian Federal University, Krasnoyarsk 660041, Russia; Institute of Computational Modelling, Federal Research Center KSC SB RAS, Krasnoyarsk 660036, Russia*

Sergey P. Polyutov − *International Research Center of Spectroscopy and Quantum Chemistry, Siberian Federal University, Krasnoyarsk 660041, Russia;* orcid.org/0000-0003-1366-1986

Sergey V. Karpov − *International Research Center of Spectroscopy and Quantum Chemistry, Siberian Federal University, Krasnoyarsk 660041, Russia; L. V. Kirensky Institute of Physics, Federal Research Center KSC SB RAS, Krasnoyarsk 660036, Russia*

Complete contact information is available at: https://pubs.acs.org/10.1021/acs.jpcc.1c01424

Notes

The authors declare no competing financial interest.

ACKNOWLEDGMENTS

The work was supported by the Russian Science Foundation (project no. 18-13-00363). L.K.S acknowledges the support of Carl Tryggers Stifetelse, project CTS 18-441.

REFERENCES

(1) Shvets, G.; Tsukerman, I. *Plasmonics and Plasmonic Metamaterials: Analysis and Applications*; World Scientific, 2012; Vol. 4.

(2) Panneerselvam, R.; Liu, G.-K.; Wang, Y.-H.; Liu, J.-Y.; Ding, S.-Y.; Li, J.-F.; Wu, D.-Y.; Tian, Z.-Q. Surface-enhanced Raman spectroscopy: bottlenecks and future directions. *Chem. Commun.* **2018**, *54*, 10−25.

(3) Sun, G.; Khurgin, J. *Plasmonics and Plasmonic Metamaterials*; World Scientific, 2011.
(4) Schasfoort, R. B. *Handbook of Surface Plasmon Resonance*; Royal Society of Chemistry, 2017.
(5) Amendola, V.; Pilot, R.; Frasconi, M.; Maragò, O. M.; Iatì, M. A. Surface plasmon resonance in gold nanoparticles: a review. *J. Phys.: Condens. Matter* **2017**, *29*, 203002.
(6) Stockman, M. I. Nanoplasmonics: past, present, and glimpse into future. *Opt. Express* **2011**, *19*, 22029−22106.
(7) Chateau, D.; Liotta, A.; Vadcard, F.; Navarro, J. R. G.; Chaput, F.; Lermé, J.; Lerouge, F.; Parola, S. From gold nanobipyramids to nanojavelins for a precise tuning of the plasmon resonance to the infrared wavelengths: experimental and theoretical aspects. *Nanoscale* **2015**, *7*, 1934−1943.
(8) Morton, S. M.; Silverstein, D. W.; Jensen, L. Theoretical Studies of Plasmonics using Electronic Structure Methods. *Chem. Rev.* **2011**, *111*, 3962−3994.
(9) Stöckle, R. M.; Suh, Y. D.; Deckert, V.; Zenobi, R. Nanoscale chemical analysis by tip-enhanced Raman spectroscopy. *Chem. Phys. Lett.* **2000**, *318*, 131−136.
(10) Thakor, A. S.; Jokerst, J.; Zavaleta, C.; Massoud, T. F.; Gambhir, S. S. Gold Nanoparticles: A Revival in Precious Metal Administration to Patients. *Nano Lett.* **2011**, *11*, 4029−4036.
(11) Huang, X.; Jain, P. K.; El-Sayed, I. H.; El-Sayed, M. A. Gold nanoparticles: interesting optical properties and recent applications in cancer diagnostics and therapy. *Nanomedicine* **2007**, *2*, 681−693.
(12) Navarro, J. R. G.; Lerouge, F.; Cepraga, C.; Micouin, G.; Favier, A.; Chateau, D.; Charreyre, M.-T.; Lanoë, P.-H.; Monnereau, C.; Chaput, F.; et al. Nanocarriers with ultrahigh chromophore loading for fluorescence bio-imaging and photodynamic therapy. *Biomaterials* **2013**, *34*, 8344−8351.
(13) Glembocki, O.; Prokes, S.; Szmacinski, H.; Liu, J.; Kub, F.; Kub, C. Nanoshell, nanosphere, and nanowire geometries for hot spot formation in surface enhanced Raman scattering. *Nanosensing: Materials and Devices II*; SPIE, 2005; p 600809.
(14) Duan, S.; Tian, G.; Ji, Y.; Shao, J.; Dong, Z.; Luo, Y. Theoretical modeling of plasmon-enhanced Raman images of a single molecule with subnanometer resolution. *J. Am. Chem. Soc.* **2015**, *137*, 9515−9518.
(15) Anger, P.; Bharadwaj, P.; Novotny, L. Enhancement and quenching of single-molecule fluorescence. *Phys. Rev. Lett.* **2006**, *96*, 113002.
(16) Saute, B.; Narayanan, R. Solution-based direct readout surface enhanced Raman spectroscopic (SERS) detection of ultra-low levels of thiram with dogbone shaped gold nanoparticles. *Analyst* **2011**, *136*, 527−532.
(17) Le Ru, E. C.; Grand, J.; Sow, I.; Somerville, W. R. C.; Etchegoin, P. G.; Treguer-Delapierre, M.; Charron, G.; Félidj, N.; Lévi, G.; Aubard, J. A Scheme for Detecting Every Single Target Molecule with Surface-Enhanced Raman Spectroscopy. *Nano Lett.* **2011**, *11*, 5013−5019.
(18) Kostyukov, A. S.; Ershov, A. E.; Gerasimov, V. S.; Filimonov, S. A.; Rasskazov, I. L.; Karpov, S. V. Super-efficient laser hyperthermia of malignant cells with core-shell nanoparticles based on alternative plasmonic materials. *J. Quant. Spectrosc. Radiat. Transfer* **2019**, *236*, 106599.
(19) Halas, N. J. Plasmonics sheds light on the nanotechnology of daguerreotypes. *Proc. Natl. Acad. Sci. U.S.A.* **2019**, *116*, 13724−13726.
(20) Linic, S.; Christopher, P.; Ingram, D. B. Plasmonic-metal nanostructures for efficient conversion of solar to chemical energy. *Nat. Mater.* **2011**, *10*, 911−921.
(21) Dhand, C.; Dwivedi, N.; Loh, X. J.; Jie Ying, A. N.; Verma, N. K.; Beuerman, R. W.; Lakshminarayanan, R.; Ramakrishna, S. Methods and strategies for the synthesis of diverse nanoparticles and their applications: a comprehensive overview. *RSC Adv.* **2015**, *5*, 105003−105037.
(22) Yang, G. Laser ablation in liquids: Applications in the synthesis of nanocrystals. *Prog. Mater. Sci.* **2007**, *52*, 648−698.
(23) Lorazo, P.; Lewis, L. J.; Meunier, M. Short-pulse laser ablation of solids: from phase explosion to fragmentation. *Phys. Rev. Lett.* **2003**, *91*, 225502.
(24) Tsuji, T.; Thang, D.-H.; Okazaki, Y.; Nakanishi, M.; Tsuboi, Y.; Tsuji, M. Preparation of silver nanoparticles by laser ablation in polyvinylpyrrolidone solutions. *Appl. Surf. Sci.* **2008**, *254*, 5224−5230.
(25) Tsuji, T.; Okazaki, Y.; Tsuboi, Y.; Tsuji, M. Nanosecond Time-Resolved Observations of Laser Ablation of Silver in Water. *Jpn. J. Appl. Phys.* **2007**, *46*, 1533−1535.
(26) DeVetter, B. M.; Bernacki, B. E.; Bennett, W. D.; Schemer-Kohrn, A.; Alvine, K. J. Fabrication of Periodic Gold Nanocup Arrays Using Colloidal Lithography. *J. Visualized Exp.* **2017**, *127*, No. e56204.
(27) Tan, B. J. Y.; Sow, C. H.; Koh, T. S.; Chin, K. C.; Wee, A. T. S.; Ong, C. K. Fabrication of Size-Tunable Gold Nanoparticles Array with Nanosphere Lithography, Reactive Ion Etching, and Thermal Annealing. *J. Phys. Chem. B* **2005**, *109*, 11100−11109.
(28) Brodoceanu, D.; Fang, C.; Voelcker, N. H.; Bauer, C. T.; Wonn, A.; Kroner, E.; Arzt, E.; Kraus, T. Fabrication of metal nanoparticle arrays by controlled decomposition of polymer particles. *Nanotechnology* **2013**, *24*, 085304.
(29) Kuo, C.-W.; Shiu, J.-Y.; Cho, Y.-H.; Chen, P. Fabrication of Large-Area Periodic Nanopillar Arrays for Nanoimprint Lithography Using Polymer Colloid Masks. *Adv. Mater.* **2003**, *15*, 1065−1068.
(30) Loza, K.; Heggen, M.; Epple, M. Synthesis Structure, Properties, and Applications of Bimetallic Nanoparticles of Noble Metals. *Adv. Funct. Mater.* **2020**, *30*, 1909260.
(31) Sørensen, L. K.; Utyushev, A. D.; Zakomirnyi, V. I.; Ågren, H. Atomistic description of plasmonic generation in alloys and core shellnanoparticles. *Phys. Chem. Chem. Phys.* **2021**, *1*, 173−185.
(32) Slaughter, L. S.; Chang, W.-S.; Swanglap, P.; Tcherniak, A.; Khanal, B. P.; Zubarev, E. R.; Link, S. Single-Particle Spectroscopy of Gold Nanorods beyond the Quasi-Static Limit: Varying the Width at Constant Aspect Ratio. *J. Phys. Chem. C* **2010**, *114*, 4934−4938.
(33) Yang, B.; Chen, G.; Ghafoor, A.; Zhang, Y.; Zhang, Y.; Zhang, Y.; Luo, Y.; Yang, J.; Sandoghdar, V.; Aizpurua, J.; et al. Sub-nanometre resolution in single-molecule photoluminescence imaging. *Nat. Photonics* **2020**, *14*, 693−699.
(34) McMahon, J. M.; Gray, S. K.; Schatz, G. C. Calculating nonlocal optical properties of structures with arbitrary shape. *Phys. Rev. B: Condens. Matter Mater. Phys.* **2010**, *82*, 035423.
(35) Baxter, J.; Lesina, A. C.; Ramunno, L. Parallel FDTD modelling of nonlocality in plasmonics. *IEEE Transactions on Antennas and Propagation*; IEEE, 2020; p 1.
(36) Iida, K.; Noda, M.; Ishimura, K.; Nobusada, K. First-principles computational visualization of localized surface plasmon resonance in gold nanoclusters. *J. Phys. Chem. A* **2014**, *118*, 11317−11322.
(37) Chen, X.; Moore, J. E.; Zekarias, M.; Jensen, L. Atomistic electrodynamics simulations of bare and ligand-coated nanoparticles in the quantum size regime. *Nat. Commun.* **2015**, *6*, 8921.
(38) Zakomirnyi, V. I.; Rinkevicius, Z.; Baryshnikov, G. V.; Sørensen, L. K.; Ågren, H. The Extended Discrete Interaction Model: Plasmonic Excitations of Silver Nanoparticles. *J. Phys. Chem. C* **2019**, *123*, 28867−28880.
(39) Ringe, E.; Langille, M. R.; Sohn, K.; Zhang, J.; Huang, J.; Mirkin, C. A.; Van Duyne, R. P.; Marks, L. D. Plasmon Length: A Universal Parameter to Describe Size Effects in Gold Nanoparticles. *J. Phys. Chem. Lett.* **2012**, *3*, 1479−1483.
(40) Zakomirnyi, V. I.; Rasskazov, I. L.; Sørensen, L. K.; Carney, P. S.; Rinkevicius, Z.; Ågren, H. Plasmonic nano-shells: atomistic discrete interaction versus classic electrodynamics models. *Phys. Chem. Chem. Phys.* **2020**, *22*, 13467−13473.
(41) Navarro, J. R. G.; Lerouge, F. From gold nanoparticles to luminescent nano-objects: experimental aspects for better gold-chromophore interactions. *Nanophotonics* **2017**, *6*, 71−92.
(42) Geitner, N. K.; Doepke, A.; Fickenscher, M. A.; Yarrison-Rice, J. M.; Heineman, W. R.; Jackson, H. E.; Smith, L. M. The morphology and evolution of bipyramidal gold nanoparticles. *Nanotechnology* **2011**, *22*, 275607.

https://doi.org/10.1021/acs.jpcc.1c01424
J. Phys. Chem. C 2021, 125, 13900−13908

(43) Douglas-Gallardo, O. A.; Berdakin, M.; Frauenheim, T.; Sánchez, C. G. Plasmon-induced hot-carrier generation differences in gold and silver nanoclusters. *Nanoscale* **2019**, *11*, 8604−8615.
(44) Birge, R. R. Calculation of molecular polarizabilities using an anisotropic atom point dipole interaction model which includes the effect of electron repulsion. *J. Chem. Phys.* **1980**, *72*, 5312−5319.
(45) Thole, B. T. Molecular polarizabilities calculated with a modified dipole interaction. *Chem. Phys.* **1981**, *59*, 341−350.
(46) Jensen, L.; Åstrand, P.-O.; Sylvester-Hvid, K. O.; Mikkelsen, K. V. Frequency-Dependent Molecular Polarizability Calculated within an Interaction Model. *J. Phys. Chem. A* **2000**, *104*, 1563−1569.
(47) Olson, M. L.; Sundberg, K. R. An atom monopole-dipole interaction model with charge transfer for the treatment of polarizabilities of π-bonded molecules. *J. Chem. Phys.* **1978**, *69*, 5400−5404.
(48) Grimme, S.; Antony, J.; Ehrlich, S.; Krieg, H. A consistent and accurate ab initio parametrization of density functional dispersion correction (DFT-D) for the 94 elements H-Pu. *J. Chem. Phys.* **2010**, *132*, 154104.
(49) Schwerdtfeger, P.; Nagle, J. K. Table of static dipole polarizabilities of the neutral elements in the periodic table. *Mol. Phys.* **2018**, *117*, 1200−1225.
(50) Zhu, S.; Chen, T. P.; Liu, Y. C.; Liu, Y.; Fung, S. A quantitative modeling of the contributions of localized surface plasmon resonance and interband transitions to absorbance of gold nanoparticles. *J. Nanoparticle Res.* **2012**, *14*, 856.
(51) Mayer, A. Formulation in terms of normalized propagators of a charge-dipole model enabling the calculation of the polarization properties of fullerenes and carbon nanotubes. *Phys. Rev. B: Condens. Matter Mater. Phys.* **2007**, *75*, 045407.
(52) Baker, A. H.; Jessup, E. R.; Manteuffel, T. A Technique for Accelerating the Convergence of Restarted GMRES. *SIAM J. Matrix Anal. Appl.* **2005**, *26*, 962−984.
(53) Landau, L. D.; Pitaevskii, L. P.; Lifshitz, E. M. *Electrodynamics of Continuous Media (Course of Theoretical Physics)*, 2nd ed.; Butterworth-Heinemann, 1984; Vol. *8*.
(54) Jensen, L. L.; Jensen, L. Electrostatic Interaction Model for the Calculation of the Polarizability of Large Noble Metal Nanoclusters. *J. Phys. Chem. C* **2008**, *112*, 15697−15703.
(55) Schroeder, W.; Martin, K.; Lorensen, B. *The Visualization Toolkit*, 4th ed.; Kitware, 2006.
(56) Ayachit, U. *The ParaView Guide (Full Color Version): A Parallel Visualization Application*; Kitware: Incorporated, 2015.
(57) Lumerical Solutions. FDTD Solutions. 2020. www.lumerical.com/tcad-products/fdtd/, accessed 30 Jan 2021.
(58) Quinten, M. Local fields close to the surface of nanoparticles and aggregates of nanoparticles. *Appl. Phys. B* **2001**, *73*, 245−255.
(59) Lee, G. J.; Kim, J. J.; Hwangbo, C. K.; Kim, J.; Park, I.; Lee, Y. P. Optical Properties of Ag Hemisphere-like Nanoparticles. *J. Nanosci. Nanotechnol.* **2013**, *13*, 568−571.
(60) Mary, A.; Koller, D. M.; Hohenau, A.; Krenn, J. R.; Bouhelier, A.; Dereux, A. Optical absorption of torus-shaped metal nanoparticles in the visible range. *Phys. Rev. B: Condens. Matter Mater. Phys.* **2007**, *76*, 245422.
(61) Aizpurua, J.; Hanarp, P.; Sutherland, D. S.; Käll, M.; Bryant, G. W.; García de Abajo, F. J. Optical Properties of Gold Nanorings. *Phys. Rev. Lett.* **2003**, *90*, 057401.
(62) Krajczewski, J.; Kołątaj, K.; Kudelski, A. Plasmonic nanoparticles in chemical analysis. *RSC Adv.* **2017**, *7*, 17559−17576.
(63) Ye, S.; Marston, G.; McLaughlan, J. R.; Sigle, D. O.; Ingram, N.; Freear, S.; Baumberg, J. J.; Bushby, R. J.; Markham, A. F.; Critchley, K.; et al. Engineering Gold Nanotubes with Controlled Length and Near-Infrared Absorption for Theranostic Applications. *Adv. Funct. Mater.* **2015**, *25*, 2117−2127.
(64) Liu, Y.-l.; Zhu, J.; Weng, G.-j.; Li, J.-j.; Zhao, J.-w. Gold nanotubes: synthesis, properties and biomedical applications. *Microchim. Acta* **2020**, *187*, 612.
(65) Chen, J.; Saeki, F.; Wiley, B. J.; Cang, H.; Cobb, M. J.; Li, Z.-Y.; Au, L.; Zhang, H.; Kimmey, M. B.; Li, X.; et al. Gold Nanocages: Bioconjugation and Their Potential Use as Optical Imaging Contrast Agents. *Nano Lett.* **2005**, *5*, 473−477.

https://doi.org/10.1021/acs.jpcc.1c01424
J. Phys. Chem. C 2021, 125, 13900−13908